Advances in Geo-Energy Research

Original article

A study of correlation between permeability and pore space based on dilation operation

Wenshu Zha[1], Shu Yan[2], Daolun Li[1]*, Detang Lu[3]

[1]*School of Mathematics, Hefei University of Technology, Hefei 230009, P. R. China*

[2]*Daqing Well Logging Technology Service Company, Daqing 163453, P. R. China*

[3]*School of Engineering, University of Science and Technology of China, Hefei 230026, P. R. China*

Abstract: CO_2 and fracturing liquid injection into tight and shale gas reservoirs induces reactivity between minerals and injected materials, which results in porosity change and thus permeability change. In this paper, the dilation operation is used to simulate the change of the porosity and the corresponding change of permeability based on Lattice-Boltzmann is studied. Firstly we obtain digital images of a real core from CT experiment. Secondly the pore space of digital cores is expanded by dilation operation which is one of basic mathematical morphologies. Thirdly, the distribution of pore bodies and pore throats is obtained from the pore network modeling extracted by maximal ball method. Finally, the correlation between network modeling parameters and permeabilities is analyzed. The result is that the throat change leads to exponential change of permeability and that the big throats significantly influence permeability.

Keywords: Permeability, pore space change, dilation operation, pore network model, microscopic percolation.

1. Introduction

Concerns over greenhouse gas emissions are leading to the investigation and realization of carbon storage in recent years. The capture and geological storage of CO_2 is a viable strategy to reduce the release of greenhouses gases to the atmosphere. CO_2 injection into oil reservoirs has been widely accepted as an effective technique for enhanced oil recovery (EOR), and has been used by the oil industry for over many years (Jessen et al., 2005). The injection of CO_2 into the deep oil reservoirs will result in chemical disequilibria and the initiation of various chemical reactions (Czernichowski-Lauriol et al., 2006). The reactions result in modification of porosities and permeabilities, which influence the actual injection and migration of CO_2.

Shale gas reservoirs are so tight that slip flow and Knudsen diffusion cannot be neglected (Li et al., 2016a; Li et al., 2016b). During the development of the tight and shale gas and oil reservoirs, hydraulic fracturing is always conducted to improve conductivity of reservoirs. Many materials in the fracturing liquid induce reactivity and cause the modification of pore diameters.

The oil reservoirs typically extend over a large area, possibly several hundred kilometers across and are developed by the natural drives or by injecting water or gas. The ultimate success of an oil recovery scheme is the result of countless displacement events at a micron-sized or nanometer-sized scale. The advances in micro-imaging of natural rocks, combined with the advances in pore-network modeling, allow researchers to gain a better understanding of pore-level displacement mechanisms.

Microscopic percolation flow is to study the flow mechanism in porosity media on pore-scale mainly by experimental simulation and numerical simulation (Blunt et al., 1990; Lindquist et al., 1996; Bakke et al. 1997; Liang et al., 1998; Blunt et al., 2002; Silin et al., 2006; Al-Kharusi et al. 2007; Dong et al., 2009). By using CT experiment of real core with X-ray, the three-dimensional volume data of rock are acquired with the micron resolution. The microscopic structure of the pore space can be obtained using the algorithm of pore-network modeling from the volume data. In the pore

---

*Corresponding authors. Email: ldaol@hfut.edu.cn.
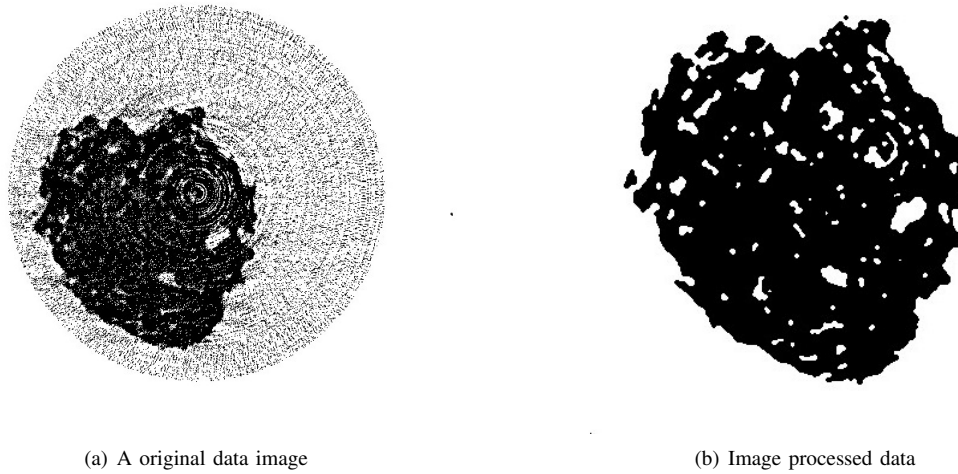
(a) A original data image

(b) Image processed data

Fig. 1. Image Processing.

network model, pore bodies represent the spacious part of pore space and throats represent the long-narrow part of pore space. Various characteristics can be predicted during fluid flow based on the pore network model (Bakke et al., 1997; Dixit et al., 1998; Blunt et al., 2002; ∅ren et al., 2002).

There are many methods to reconstruct the pore network. The major methods include the medial axis based method and maximal ball method. Medial axis method uses image processing to subtract the medial axis to represent the topological skeleton of pore space (Liang et al., 1998; Lindquist et al., 1996). The maximal ball (Al-Kharusi et al., 2007; Dong et al., 2009; Silin et al., 2006) method try to find the largest spheres centered on each voxel in the pore space. Maximal method first is proposed by Silin, and then extended by Donghu and Blunt. The method of the pore network modeling used in this paper is also extended from maximal ball method (Zhang et al., 2013). Apart from the direct method to get 3D volume data, there are many indirect ways to generate the pore space, such as the statistical model (Okabe et al., 2005; Zhang et al., 2010) and process stimulating method (∅ren et al., 2002).

In this paper, we first do CT experiment of nature core and get 118 slices of digital images with the 10-micron resolution. Dilation operation, one of basic mathematical morphologies, is used to simulate the increasing of porosity when acidic fluid is injected into oil reservoir. At last, we calculate the permeability of every digital core by Lattice-Boltzmann and analyze on the correlation between model parameters and permeability.

2. Core's CT experiment and image processing

2.1 The principle and device of CT experiment

CT experiment is based on the interaction between ray and sample. Different substance in the sample has different absorption coefficient. When ray passes through some substance, its intensity can be expressed by:

$$I = I_0 e^{-\Sigma u_i D_i} \tag{1}$$

where u_i is decline coefficient of different substance, D_i is thickness of substance. Because the different absorption coefficient of pore and frame in porous media, we can get the inner structure of core by CT experiment.

The projection data of different angle can be expressed by:

$$p_\phi(x_r) = \int_L u(x,y)dl = \ln(I_{0\phi}(x_r)/I_\phi(x_r)) \tag{2}$$

where ϕ is projection angle, X_r is coordinates of ray, L is path of ray's pass through sample. The projection data can be calculated by Eq. (2), then use CT reconstruction algorithm to calculate u(x,y).

Our experiment was done in Beijing Synchrotron Radiation Facility. The light source is X-ray, scanner system gets one projection image every one degree. The image collection system uses CCD whose resolution is 10μm. The experimental sample is a cylindrical sandstone core with a diameter of 3mm.

2.2 Image processing

The original images obtained from CT experiment are grayscale images and image processing is needed. After noise removal, image enhancement and image segmentation, the grayscale images are turned into binary images, in which each voxel is represented by a single bit, being 1 for pore and 0 for solid (see Fig. 1).

It is either costly or unavailable to obtain the experimental data of a rock before and after flooding by CO_2 or acidic fluid at the millimeter-sized scale. Therefore the digital image processing technique is used to approximately simulate the change of pore space caused by the chemical reaction.

2.3 Basic morphological operations: erosion and dilation

The basic morphological operations, erosion and dilation, can change the size of objects when applied to either grayscale
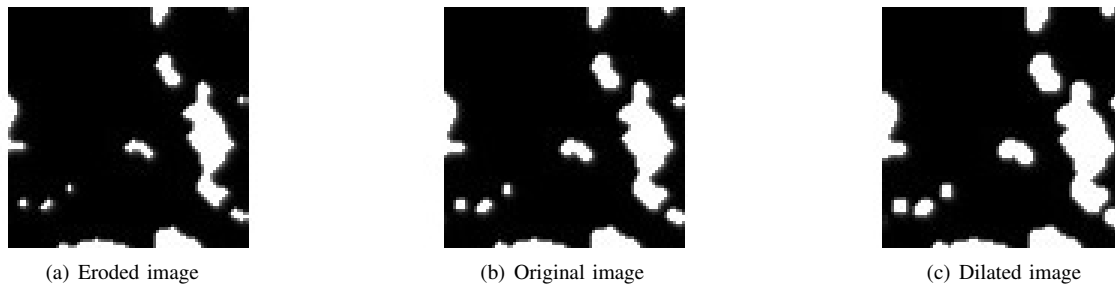
(a) Eroded image   (b) Original image   (c) Dilated image

Fig. 2. Eroded and dilated images, white color represents pore space.

or binary images. Erosion shrinks image objects while dilation expands them.

The characteristics of erosion are that erosion generally decreases the sizes of objects and removes small anomalies by subtracting objects with a radius smaller than the structuring element. So erosion is used to stimulate the decrease of the pore space.

On the contrary, dilation is to increase the sizes of objects. With binary images, dilation adds pixels to the perimeter of each image object. So dilation is used to stimulate the increase of the pore space.

The number of pixels added or removed from the objects in an image depends on the size and shape of the structuring element used to process the image. A structuring element is a matrix consisting of only 0's and 1's that can have any arbitrary shape and size.

Two-dimensional structuring elements are typically much smaller than the image being processed. A square structuring element used here is a 2×2 matrix:

$$P = \begin{bmatrix} 1 & 1 \\ 1 & 1 \end{bmatrix}$$

Figure 2 shows the original image (see Fig. 2b), the corresponding eroded image (see Fig. 2a) and corresponding dilated image (see Fig. 2c).

2.4 Three digital cores generated by erosion operation

Erosion decreases porosity while dilation increases porosity. In this sense, erosion is contrary to the dilation. So we use dilation to simulate the modification of pore space.

The whole digital core consists of a huge number of voxels. A simulation with so many voxels based on Lattice-Boltzmann would be a challenge for a computer. Therefore, only 80 serial binary images of pore space and $80 \times 80 \times 80$ pixels are combined to a 3D matrix of voxels.

Three other types of digital cores are generated by the dilation operation based on the original $80 \times 80 \times 80$ digital core. The first type is that the previous 20 serial binary images are dilated while other sixty images are not, which is marked as "20d". The second type is that only previous 40 serial binary images are dilated and marked as "40d". The third type is that only 60 serial binary images are dilated and marked as "60d". The original image is marked as "0d".

Because dilation can increase the porosity, the porosities increase gradually from "0d" digital cores, "20d" digital cores, "40d" digital cores to "60d" digital cores. Therefore the process of acidic fluid interact with the solid is approximately simulated.

Table 1 gives the porosity of 4 types of digital cores. It shows that the porosity increase linearly from 0.1705 to 0.2050, which is also shown in Figure 5.

Table 1. Distribution of radius of pore body.

Sample No	0d	20d	40d	60d
Porosity	0.1705	0.1803	0.1915	0.2050

3. Pore network modeling reconstruction method

The pore space of porous media is complex, localized disordered and not a simple geometric body. For simplification the pore space is always replaced by some kind of simple objects. In this paper, we consider the pore body as sphere and the throat as cylinder to construct the pore network modeling.

In the discrete space the concept of sphere is a little different from the concept of sphere in the continuous space. Figure 3 gives the circle with radius of 1 to radius 3.

There are many pore network modeling methods to distinguish between the pore bodies and pore throats, and establish their respective volume and connectivity. The main steps of the algorithm are as follows.

The first step is to divide original pore space into sphere pore bodies which are not included and disjointed by each other, and save the information of each sphere with the centers and radius for next step calculation.

The second step is to search and reconstruction of throat. The throat is considered to be a long-narrow space that connects two pore bodies, and it is also the channel in which fluid flow from one pore body to another. The throat can be constructed by searching the connected path between two pore neighboring bodies. The cross section area of throat can be considered as the narrowest area of channel, and will be used to define the radius of the throat.

As the throat is simplified as a cylinder and the section of the cylinder is circle, the radius of throat is calculated by the formula below
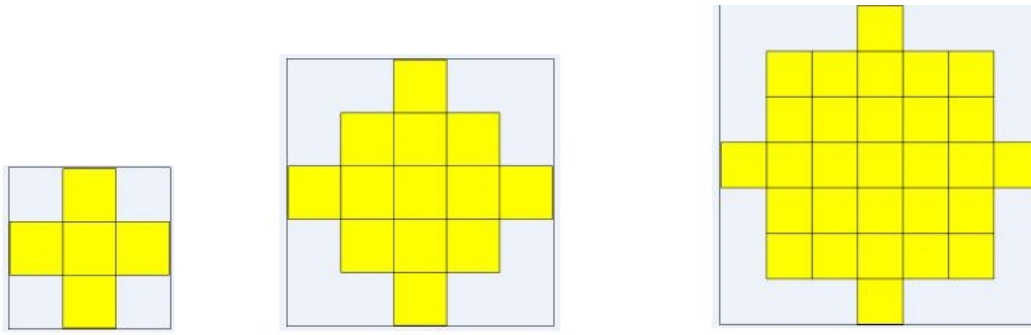
Fig. 3. Plane view of pore body with different radius (from left to right, r=1, r=2, r=3).

Table 2. Distribution of radius of pore body.

	0d	20d	40d	60d
The number of pore body with radius of 5	3	4	5	8
The number of pore body with radius of 4	25	26	31	38
The number of pore body with radius of 3	21	23	26	29
The number of pore body with radius of 2	394	407	422	418

$$\pi r^2 = width \qquad (3)$$

where r is the radius of the circle, and $width$ is the section area of a throat. Because the shape of the throat is very complex, the radius of throats is an approximate value.

4. Reconstruction result

4.1 The distribution of pore body's radius

Import the three dilated and the original digital cores and reconstruct them with pore network model. The distribution of pore body radius could describe spacious space of pore. The reconstruction result of pore body is shown in Table 2.

Table 2 shows that the number of pore bodies with radius of 3, 4 and 5 increases when more images are dilated. It shows that there are bigger pore bodies in digital cores with more dilated images.

The columns of Table 2 show that as the radius of sphere increases the number of sphere pore body decreases dramatically. It shows that most of the space is small pore particle in porous media.

4.2 Distribution of throat radius

After reconstruction of sphere pore body, the pore throats are searched and constructed. The number of throats of different radius is counted as follow:
If the section area of a throat is in the interval [29, 53], the radius of the throat is 3;
If the section area of a throat is in the interval [14, 28], the radius of the throat is 2;
If the section area of a throat is in the interval [5, 13], the radius of the throat is 1;

If the section area of a throat is in the interval [1, 4], the radius of the throat is less than 1, marked as 0.5;
The number of the throats is given in table 3.

Table 3. Distribution of pore throat.

	0d	20d	40d	60d
Radius = 3	4	4	5	10
Radius = 2	12	14	17	22
Radius = 1	174	199	202	205
Radius < 1	496	530	537	544

Table 3 shows that when more images are dilated, the radii of throats increase. The "0d" digital core and the "20d" digital core have equal number of pore throats with radius of 3, which means that the largest pore throat does not exit in previous 20 images.

The distribution of the number of throats with different radii is also shown in Figure 4, which apparently shows that the number of throat decreases greatly when the radius of throat increases.

5. Permeability calculation and analysis

5.1 Permeability calculation with LBM method

There are two types of models to simulate flow in porous media at pore scale. One is network flow modeling and another is Lattice-Boltzmann. Lattice-Boltzmann is adopted to simulate flow and calculate the absolute permeabilities of four digital core samples in order to analyze the correlation between network model parameters and permeabilities. Here
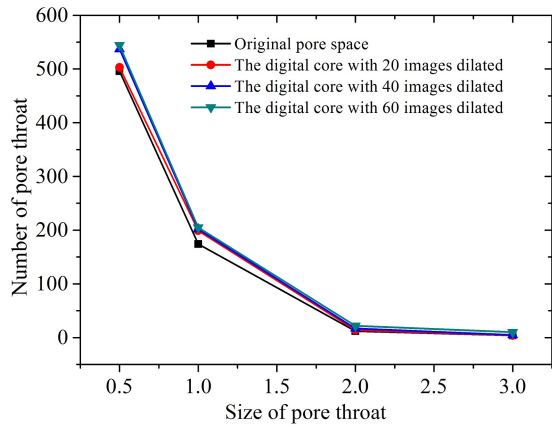
Fig. 4. Distribution of throat.

D3Q19 model (Maier et al., 1996) is used and its evolution equation is:

$$f_i(x + \Delta x, t + \Delta t) = f_i(x,t) - \frac{1}{\tau}(f_i(x,t) - f_i^{eq}(x,t)) \quad (4)$$

where $f_i(x,t)$ is distribution function at time t, location x and direction i. $f_i^{eq}(x,t)$ is equilibrium distribution function, it can be described as:

$$f_i^{eq}(x,t) = w_i\rho[1 + 3\frac{e_i u}{c^2}] + 4.5\frac{e_i u}{c^4} - 1.5\frac{u^2}{c^2}] \quad (5)$$

w_i is weight value, e_i is discrete velocity. They can be expressed as follows:

$$w_i = \begin{cases} 1/3, & i = 0 \\ 1/18, & i = 1, 2 \cdots 6 \\ 1/36, & i = 7, \cdots 18 \end{cases} \quad (6)$$

$$e_i = \begin{cases} (0,0,0) & i = 0 \\ (\pm1,0,0),(0,\pm1,0),(0,0,\pm1) & i = 1, 2 \cdots 6 \\ (\pm1,\pm1,0),(\pm1,0,\pm1),(0,\pm1,\pm1) & i = 7, \cdots 18 \end{cases} \quad (7)$$

The density and momentum of fluid can be expressed by:

$$\rho = \Sigma f_i(x,t) \quad (8)$$

$$\rho u = \Sigma f_i(x,t)e_i \quad (9)$$

5.2 The relationship between permeabilities and other porous media parameters

There are many porous media parameters such as porosity, coordination number, the distribution of pore body and throat. The coordination number of a pore body is the number of

pore throats connecting it to other pore bodies. It is one of important parameters of pore space because the connections of pore throat control the flow properties. Since the four types of the digital cores almost have the same morphologies, the analysis of coordination number is neglected.

As definition of pore network model, a complete flow channel consists of two elements, pore body and throat. Pore throats are the narrow flow channels that connect the pore bodies and determine the rock permeabilities. The pore body is spacious pore space for storing fluid. Generally, pore bodies determine the rock porosity. Therefore the analysis of the relation between permeabilities and pore bodies is omitted.

5.3 The relationship between permeabilities and porosities

The permeability is calculated by above mentioned LBM method. In order to observe the effect of porosity on permeability, we sort the four samples according to the porosities. The order is "0d" digital core, "20d" digital core, "40d" digital core, "60d" digital core, shown as Figure 5.
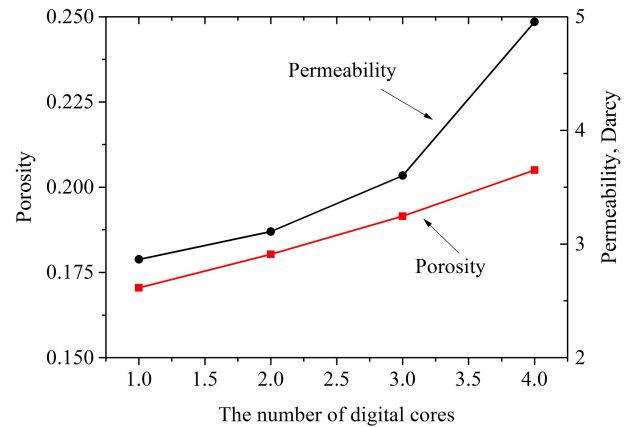

Fig. 5. Relationship between the permeabilities and the porosities.

As showed in Figure 5, permeabilities go up as porosities increase. Although the increasing trend is same, the increasing rates have a big difference. The porosity increases linearly while the permeability increases exponentially. It shows that porosity is not the main influencing factor on permeability.

5.4 Distribution of throat radius

The permeabilities and the number of throats for all samples are shown in Figure 6, where the number of throats with radius of 1 is minus 150 for displaying conveniently. It is to see that the curves of permeability and the curves of the number of throats with a radius of 1 have different trends, which shows that the small pore throats are not essential factor for permeabilities.

However, the curves of radii with 2 and 3 approximately coincide with the curves of permeabilities.
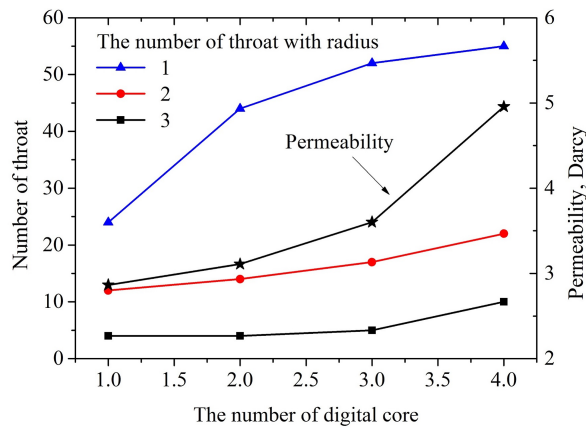
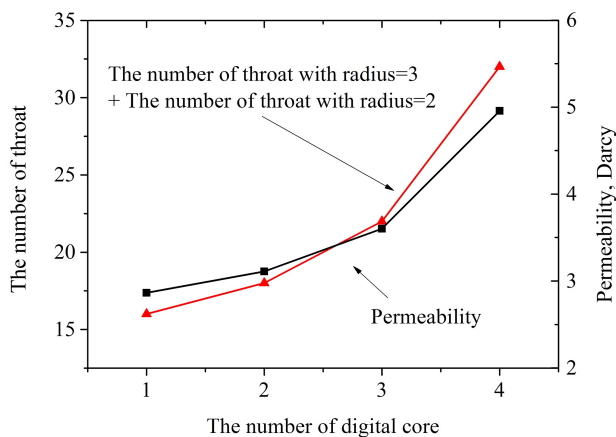**Fig. 6.** Relationship between permeability and the Number of big throats.

Fig. 7. Relationship between the permeability and the number of large pore bodies.

In order to see the correlation between big throats and permeabilities, we add the number of throats with radius of 3 and 2. The big throats and permeabilities are plotted in Figure 7 at different scale.

Figure 7 shows that the two curves have the same increase trend. The permeability increases in the same way as the number of big throats increases. It shows that permeability K is significantly determined by the number of big throats. It can be interpreted by Hagen-Poiseuille formula and the Darcy law.

In pore network model of porous media, the flow channel is composed of many cells of pore body connected by throat. Every channel can be considered as a capillary. Hagen-Poiseuille formula is:

$$Q = (P_i - P_j)\frac{\pi r^4}{8\mu L} \tag{10}$$

From the Darcy law and Hagen-Poiseuille formula, the permeability is mainly decided by r^2, therefore the big throats decide the value of the permeability.

6. Conclusions

Based on the real data getting from core's CT experiment,

we obtained the digital cores with the operation of dilation to simulate the pore space change. The corresponding permeability was calculated with LBM method.

The dilated and original digital cores have the same topological structure. Therefore, they have the same distribution of cooperation number and pore bodies, and thus the correlation between the permeability and pore throats can be exactly analyzed.

The result is that when the porosity changes, the permeability changes significantly. The trend of permeability change is agreement with the trend of the number of big throats.

References

Al-Kharusi, A.S., Blunt, M.J. Network extraction from sandstone and carbonate pore space images. J. Petrol. Sci. Eng. 2007, 56(4): 219-231.

Bakke, S., ∅ren, P. 3-D pore-scale modelling of sandstones and flow simulations in the pore networks. SPE J. 1997, 2(2): 136-149.

Blunt, M., King, P. Macroscopic parameters from simulations of pore scale flow. Phys. Rev. A 1990, 42(8): 4780.

Blunt, M.J., Jackson, M.D., Piri, M., et al. Detailed physics, predictive capabilities and macroscopic consequences for pore-network models of multiphase flow. Adv. Water Resour. 2002, 25(8): 1069-1089.

Czernichowski-Lauriol, I., Rochelle, C., Gaus, I., et al. Geochemical interactions between CO2, pore-waters and reservoir rocks. Advances in the geological storage of carbon dioxide. Dordrecht: Springer, 2006: 157-174.

Dixit, A.B., McDougall, S.R., Sorbie, K.S. A pore-level investigation of relative permeability hysteresis in water-wet systems. SPE J. 1998, 3(2): 115-123.

Dong, H., Blunt, M.J. Pore-network extraction from micro-computerized-tomography images. Phys. Rev. E 2009, 80(3): 36307.

Jessen, K., Kovscek, A.R., Orr, F.M. Increasing CO_2 storage in oil recovery. Energ. Convers. Manage. 2005, 46(2): 293-311.

Li, D., Zha, W., Liu, S., et al. Pressure transient analysis of low permeability reservoir with pseudo threshold pressure gradient. J. Petrol. Sci. Eng. 2016a, 147: 308-316.

Li, D., Zhang, L., Wang, J.Y., et al. Composition-Transient analysis in shale-gas reservoirs with consideration of multicomponent adsorption. SPE J. 2016b, 21(2): 648-664.

Zha, W., et al. Adv. Geo-energ. Res. 2017, 1(2): 93-99

99

Liang, Z.R., Fernandes, C.P., Magnani, F.S., et al. A reconstruction technique for three-dimensional porous media using image analysis and Fourier transforms. J. Petrol. Sci. Eng. 1998, 21(3): 273-283.

Lindquist, W.B., Lee, S.M., Coker, D.A., et al. Medial axis analysis of void structure in three-dimensional tomographic images of porous media. J. Geophys. Res-Sol. Ea. 1996, 101(B4): 8297-8310.

Okabe, H., Blunt, M.J. Pore space reconstruction using multiple-point statistics. J. Petrol. Sci. Eng. 2005, 46(1): 121-137.

Øren, P., Bakke, S. Process based reconstruction of sandstones and prediction of transport properties. Transport. Porous. Med. 2002, 46(2): 311-343.

Silin, D., Patzek, T. Pore space morphology analysis using maximal inscribed spheres. Physica A 2006, 371(2): 336-360.

Zhang, T., Li, D., Lu, D., et al. Research on the reconstruction method of porous media using multiple-point geostatistics. Sci. China. Phys. Mech. Astron. 2010, 53(1): 122-134.

Zhang, T., Li, D., Yang, J., et al. A study of the effect of pore characteristic on permeability with a pore network model. Petrol. Sci. Technol. 2013, 31(17): 1790-1796.